Magnetically induced hyperthermia: size-dependent heating power of γ-Fe_2O_3 nanoparticles

2008 J. Phys.: Condens. Matter 20 204133

(http://iopscience.iop.org/0953-8984/20/20/204133)

J. Phys.: Condens. Matter **20** (2008) 204133 (5pp) doi:10.1088/0953-8984/20/20/204133

Magnetically induced hyperthermia: size-dependent heating power of γ-Fe_2O_3 nanoparticles

Michael Lévy[1], Claire Wilhelm[1], Jean-Michel Siaugue[2], Olivier Horner[2], Jean-Claude Bacri[1] and Florence Gazeau[1]

[1] Laboratoire Matière et Systèmes Complexes (MSC), UMR CNRS 7057, Université Paris-Diderot, Bâtiment Condorcet-Case 7056, F-75205 Paris Cedex 13, France
[2] Laboratoire des Liquides Ioniques et Interfaces Chargées (LI2C), UMR CNRS 7612, Université Pierre et Marie Curie, Bâtiment F, 4 place Jussieu, 75005 Paris, France

E-mail: florence.gazeau@univ-paris-diderot.fr

Received 3 April 2008
Published 1 May 2008
Online at stacks.iop.org/JPhysCM/20/204133

Abstract

By combining magnetic properties with nanosized biocompatible materials, superparamagnetic nanoparticles may serve as colloidal heating mediators for cancer therapy. This unique potential has attracted attention for designing new magnetic nanoparticles with high efficiency heating properties. Their heating power under high frequency magnetic field is governed by the mechanisms of magnetic energy dissipation for single-domain particles due both to internal Néel fluctuations of the particle magnetic moment and to the external Brownian fluctuations. These mechanisms are highly sensitive to the crystal size, the particle material, and the solvent properties. Here we explore the heating properties of maghemite particles with large particle sizes, in the range 15–50 nm, synthesized through a new procedure which includes a hydrothermal process. Particle shape and size distribution, hydrodynamic volume, and magnetic anisotropy are characterized, respectively, by transmission electron microscopy, dynamic magnetically induced birefringence, and ferromagnetic resonance. Together with our previous data on low diameter particles (Fortin J P *et al* 2007 *J. Am. Chem. Soc* **129** 2628–35), this study provides the whole size dependence of heating efficiency in the range 5–50 nm and assesses the balance between Néel and Brownian contributions to thermal losses. In agreement with theoretical predictions, the heating efficiency shows a maximum for an optimal size of about 15 nm.

(Some figures in this article are in colour only in the electronic version)

1. Introduction

Current developments in nanotechnology are making possible the use of nanometric particles to generate heat under the stimulus of an external field. Nanosized heat mediators have decisive advantages over macroscopic heat sources especially for therapeutic purposes. Being available as colloidal suspensions, they can be injected into the body. They are small enough to cross biological barriers, meaning that heat can be generated very close to the target. The heat generation is proportional to the local concentration of nanofoci and is limited to the site of nanoparticle accumulation. To achieve therapeutic hyperthermia, it is thus necessary to optimize both the nanoparticle concentration in the target site and the heating power of each nanoparticle. Among nanometric heat mediators, magnetic nanoparticles are the most developed due to their ability to heat when submitted to high frequency magnetic field [1]. There are two mechanisms underlying the transformation of magnetic energy into heat. Both internal and external sources of 'friction' lead to a phase lag between the applied magnetic field and the direction of the particle's magnetic moments, thereby generating thermal losses. Internal friction of the magnetic moment inside the nanocrystal originates from anisotropy energy which tends

to orient the magnetic moment in specific directions called easy axes (Néel mechanism). External friction is due to the viscosity of the carrier fluid, impeding thermal fluctuations of the particle itself (Brownian mechanism). Characteristic times of Néel (internal) and Brownian (external) fluctuations (in comparison with the magnetic field frequency) determine the heating power of the nanoparticles. Both mechanisms depend on particle size, whereas only the Brownian contribution depends on viscosity and only the Néel contribution is tuned by the magnetic anisotropy of the material. In a recent paper, we investigated the heating power of maghemite and cobalt ferrite nanoparticles with diameters in the range 5–16 nm [2] and distinguished between Néel and Brownian contributions to heating. Here we explored iron-oxide nanoparticles with larger sizes in the range 15–50 nm, synthesized with a new procedure including an hydrothermal process. Particles size distribution and shapes were characterized by transmission electron microscopy. A calorimetric study allowed determination of the heating power of these particles in solvents of different viscosities and as a function of their size. We shed light independently on the Brownian dynamics of the particles and on their Néel relaxation by performing, respectively, dynamic magnetically induced birefringence and ferromagnetic resonance to identify magnetic anisotropy. Finally, compiling the data for nanoparticles in the small (5–10 nm) and large (15–50 nm) size range, we provide the whole size dependence of heating power of monodomain colloidal maghemite nanoparticles.

2. Materials and methods

2.1. Chemical synthesis

The magnetic dispersions used in the present work are cationic ferrofluids which are stable in acidic water (pH $\approx$ 3.0). The superparamagnetic γ-Fe_2O_3 (maghemite) particles were synthesized by alkaline coprecipitation of $FeCl_2$ and $FeCl_3$ salts, using the Massart's procedure [3]. An hydrothermal process step [4] was used during the synthesis in order to grow the nanoparticles and control their size by the pH of the autoclaved solution and the molar Fe^{3+}/Fe^{2+} ratio (paper in preparation). Briefly, the coprecipitated mixture was put in an autoclave and its pH was adjusted to the desired alkaline value with a $N(CH_3)_4OH$ solution. The autoclave was then heated at 200 °C for 2 h and slowly cooled to room temperature. The mixture was then fully oxidized to maghemite, and the obtained colloidal particles were further acidified with an HNO_3 solution and washed several times with acetone and ether. Finally, the nanoparticles were dispersed in water or in glycerol.

2.2. Transmission electron microscopy (TEM) and morphological characterization

TEM was performed on a JEOL 100 CX instrument (100 kV). On TEM pictures, the contour of each individual nanoparticle was approximated by an ellipse, with a major axis a, a minor axis b, and an eccentricity $e = \sqrt{1 - b^2/a^2}$. For each sample, 200–400 nanoparticles were analyzed. Log-normal distribution correctly fitted histograms of major and minor axes with polydispersity index σ.

2.3. Magneto-optical birefringence

The experimental set-up was previously described [5]. Briefly, the ferrofluid was probed by an He–Ne laser beam (λ = 632.9 nm) of weak power placed between a polarizer and an analyzer. Transmitted light was measured by a photodetector. When submitted to a vertical magnetic field ($H = 12\,\mathrm{kA\,m^{-1}}$), the ferrofluid acquired a birefringence, due to alignment of the optical axes of the nanoparticles along the field. This birefringence Δn ($\Delta n = n_\parallel - n_\perp$, $n_\parallel$ and $n_\perp$ being the optical indexes, respectively, in the direction of the magnetic field and perpendicular to it) induces a phase lag φ proportional to Δn. The light detected by the photodetector is proportional to $\sin^2\varphi$ and to φ^2 in the limit of small phase lag. When the magnetic field is switched off, the magnetically induced birefringence relaxes because of Brownian fluctuations of the nanoparticles in the carrier fluid. Experimentally, this relaxation is not a single exponential, but is correctly described by a stretched exponential $\Delta n \propto \exp(-(t/\tau_0)^\alpha)$, revealing a distribution of relaxation times (the smaller $\alpha < 1$, the broader the distribution). For each sample, the characteristic birefringence relaxation time τ_0 and parameter α were measured both in water and in glycerol (95%).

2.4. Ferromagnetic resonance (FMR)

Ferromagnetic resonance was performed at room temperature with a Varian 102 spectrometer working at 9.26 GHz. 2 μl of ferrofluid was inserted in a glass capillary, placed in a quartz tube in the microwave cavity. The modulation field had a frequency of 100 kHz and amplitude of 10 G. The first derivative $\mathrm{d}W/\mathrm{d}H$ of the power absorption W was recorded as a function of the applied field H in the range 0–600 mT. The resonance field H_{res} is the field for which $\mathrm{d}W/\mathrm{d}H = 0$. The width of the resonance, ΔH, was defined as the bounding peaks of the FMR spectrum. The reference resonance field for free electrons is $H_0 = \omega/\gamma = 0.33$ T, where γ is the electronic gyromagnetic ratio. In a ferro- or ferrimagnetic crystal, the magnetic moment experiences not only the external field H, but also the internal anisotropy field. For a suspension of monodomain particles with uniaxial anisotropy, the resonance field is shifted from the reference field H_0 according to $H_{\mathrm{res}} = H_0 - PH_{\mathrm{a}}$, where H_{a} is the anisotropy field and P is a weighting factor depending on the orientational distribution of the anisotropy axes of particles with respect to the external magnetizing field [6]. In a liquid suspension, the anisotropy axes are able to follow the direction of the magnetic moment, but are disoriented by thermal fluctuations. Hence the shift of resonance line from the reference field, $H_0 - H_{\mathrm{res}} = H_{\mathrm{a}}^{\mathrm{eff}}$, gives an apparent anisotropy field, which is a minimal bound for the value of anisotropy field H_{a}.

2.5. Hyperthermia measurements

The laboratory-made device used for the magnetic hyperthermia experiment was previously described in [2]. It consists of

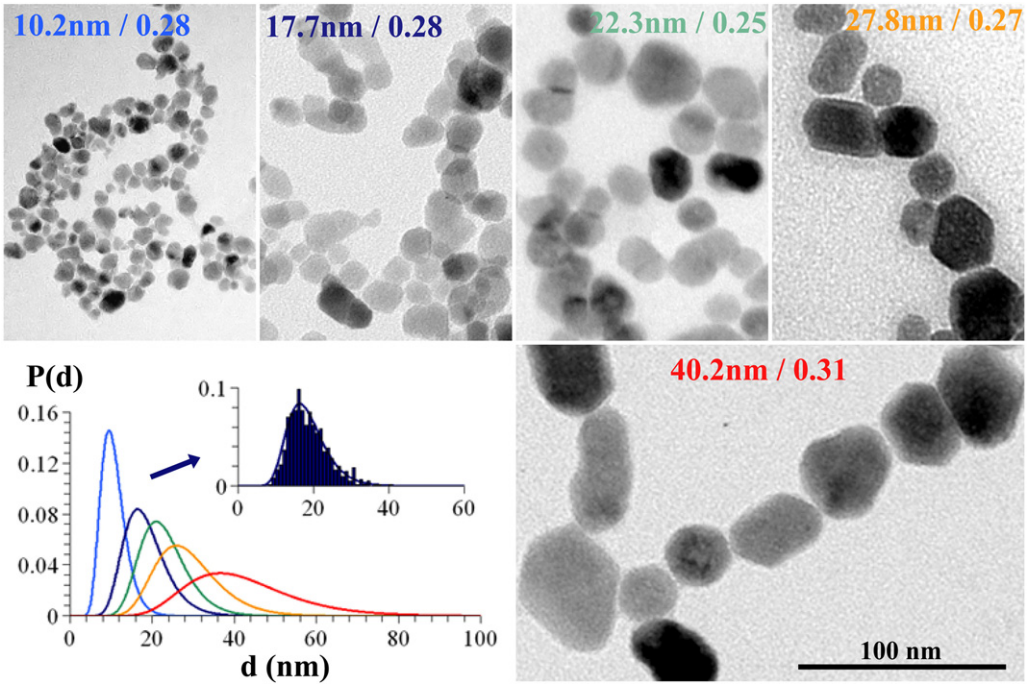

Figure 1. TEM pictures for different samples and corresponding distributions of the major axis approximated by log-normal distributions.

a resonant RLC circuit producing in a 16 mm coil a 700 kHz magnetic field with an amplitude of 27 kA m^{-1}. The coil was thermalized at 37 °C. The temperature was probed with a fluoroptic fiber thermometer. The initial linear rise of temperature as a function of time, $\frac{dT}{dt}$, was measured in order to deduce the specific loss power (SLP) of the particles defined as: SLP $= \frac{CV_s}{m}\frac{dT}{dt}$, where C is the volume specific heat capacity of the sample ($C_{water} = 4185$ J l^{-1} K^{-1}, $C_{glycerol} = 3086$ J l^{-1} K^{-1}), $V_s = 300$ μl is the sample volume, and m is the mass of iron oxide.

3. Results

3.1. Particle size distribution and shapes

All particles displayed elongated shapes with eccentricity e ranging from 0.58 to 0.7. Mean major axis and minor axis varied from 14.6 nm to 45.6 nm and from 11.63 nm to 35.7 nm respectively. As observed in figure 1, nanoparticle sizes were polydisperse, following log-normal distributions with polydispersity index from 0.24 to 0.44. For comparison, we also indicated the size distribution of one sample of smaller size [2] in the low diameter range, synthesized without the hydrothermal process.

3.2. Magneto-optical birefringence measurements

Characteristic birefringence relaxation times τ_0 are shown in figure 2(a) as a function of the mean major axis for particles dispersed in water and in glycerol. The difference of relaxation times in the two solvents was roughly proportional to the increase in viscosity. Both in water and in glycerol, τ_0 scaled with the power 3 of the major axis. Brownian relaxation time τ_B was deduced from the relationship $\tau_0 = \tau_B/2$ [7] and hydrodynamic diameter d_{hyd} from $\tau_B = \frac{3\eta V_{hyd}}{k_B T}$, where η is the viscosity, $V_{hyd} = \frac{\pi}{6} d_{hyd}^3$, k_B the Boltzmann constant, and T is the temperature. As expected, the hydrodynamic diameter increased linearly with the major axis of the particles. However, for most of the samples, the hydrodynamic diameter was larger in water than in glycerol. This suggests a better dispersion of nanoparticles in the high viscosity solvent.

3.3. Ferromagnetic resonance

Most FMR spectra presented symmetric lines, with well defined resonance field and line-width. The shift from reference field, $H_0 - H_{res} = H_a^{eff}$, representing a lower value of anisotropy field, is shown in figure 3(a) as a function of the major axis of particles. The apparent anisotropy field increased from 600 to 1700 G for particle major axes from 15 to 45 nm. For comparison, the apparent anisotropy fields of low diameter particles are also indicated, ranging from 100 to 400 G. As with the apparent anisotropy field, the line-width (figure 4(b)) increased with particle sizes from 600 to 2700 G.

The increase of apparent anisotropy field with particle size can be partly explained by the variation of the orientational distribution of anisotropy axes $\vec{n}$, assuming a constant anisotropy field. The apparent anisotropy field in the FMR spectrum should match the actual anisotropy field for anisotropy axes perfectly aligned in the direction of the applied field. However, due to thermal fluctuations, the orientational dispersion of the anisotropy axis reduces the apparent anisotropy field [6]. The larger the particle volume and its anisotropy energy, the smaller the deviation of the anisotropy axis from the direction of the applied field. In [2], a volume anisotropy energy with anisotropy constant $K = 1.6 \times 10^4$ J m^{-3} was found to fit the results of

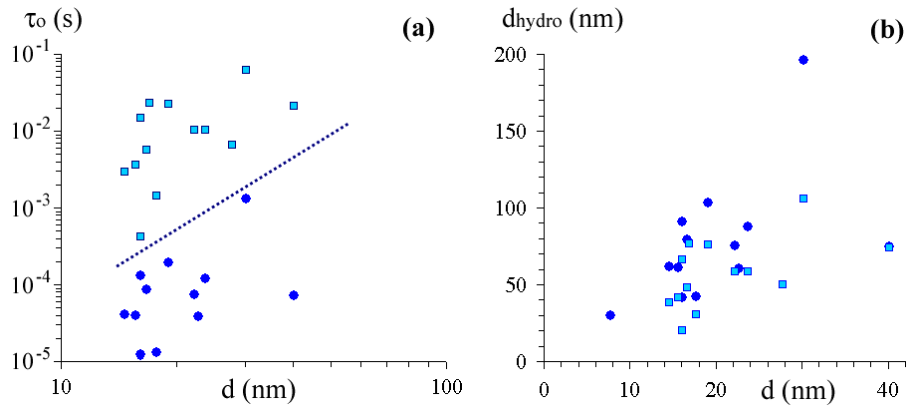

Figure 2. Characteristic birefringence relaxation time τ_0 (a) and hydrodynamic diameter $d_{\rm hyd}$ (b) as a function of mean major axis for particles dispersed in water (•) and in glycerol (■). In the log–log plot in (a), the straight line of slope 3 is an indication of the theoretical dependence of τ_0 on particle diameter.

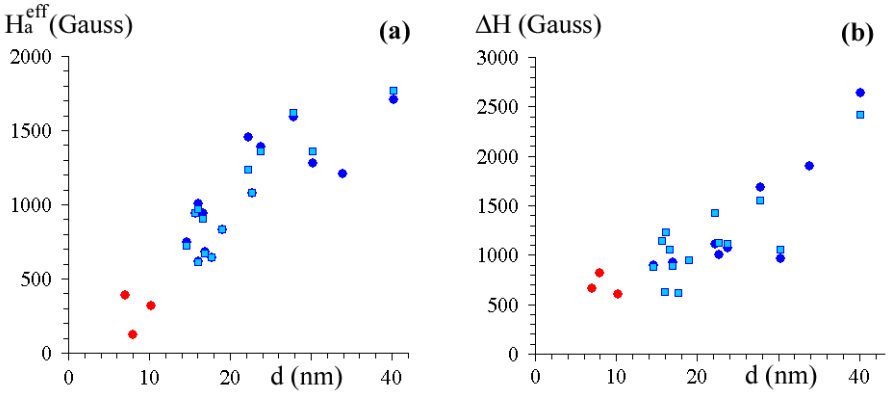

Figure 3. Ferromagnetic resonance: shift from reference field $H_0 - H_{\rm res} = H_{\rm a}^{\rm eff}$ (a) and line-width ΔH (b) of the FMR resonance line as a function of mean major axis. Results for newly synthesized high diameter samples (in blue, •, ■) and for low diameter samples (in red $d < 12$ nm, •) are compared.

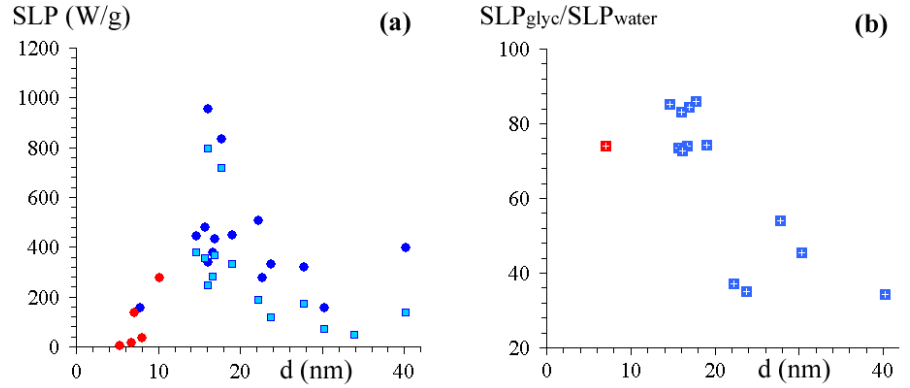

Figure 4. Heating efficiency: (a) specific loss power of samples in water (dark blue, •) and in glycerol (clear blue, ■) as a function of mean major axis. Results from [2] for low diameter particles in water (in red $d < 12$ nm, •) are also displayed. (b) Ratio of specific loss power in glycerol over specific loss power in water as a function of mean major axis.

hyperthermia measurements for low diameter particles. This corresponded to an anisotropy field of 1140 G. Such a value is consistent with FMR measurements for particle sizes up to 20 nm. However, beyond this size, the enhancement of the apparent anisotropy field reveals additional sources of anisotropy energy. Such additional contributions to anisotropy energy could also account for the very large FMR line-width of high diameter nanoparticles.

3.4. Hyperthermia measurements

The SLP values of the high diameter nanoparticles dispersed in water and in glycerol are represented in figure 4(a) as a function

of mean major axis. For comparison, results for low diameter samples are also indicated. A nonmonotonous dependence of heating power on particle size is observed. As detailed in [2], SLP strongly increased with increasing diameter from 5 to 10 nm. Maximum SLPs of 950 and 833 W g^{-1} of iron were found for two samples with the major axis distribution centered on about 16 nm. Particles with a higher major axis showed SLP between 200 and 400 W g^{-1}, with a clear decrease of heating power with increasing size.

Figure 4(b) shows the ratio of SLP measured in glycerol over SLP measured in water as a function of mean major axis. For given nanoparticles, the Néel contribution to heating power is identical in water and in glycerol, since Néel internal fluctuations are insensitive to solvent viscosity. By contrast, enhancing viscosity slows the Brownian relaxation as observed in figure 2(a) and consequently reduces the Brownian contribution to heating. Therefore the ratio of SLP in glycerol and in water represents the relative Néel contribution to heating power. As shown in figure 4(b), the Néel contribution appeared to diminish with increasing particle size, until representing only 30% of the SLP in water.

4. Discussion and conclusion

The heating efficiency of magnetic nanoparticles in an alternating magnetic field depends on the dynamic behavior of their magnetic moment, which is governed by thermal fluctuations. Internal Néel fluctuations of the magnetic moment μ relative to the crystal lattice are hindered by the anisotropy energy. The characteristic time of Néel fluctuations grows exponentially with the ratio of the anisotropy energy $\vec{\mu} \cdot \vec{H}_a$ over the thermal energy $k_B T$. By contrast, Brownian relaxation time increases linearly with the hydrodynamic volume of the particle and with the solvent viscosity. SLP of particles with known Néel and Brownian relaxation times can be predicted by using a linear response model [1, 8]. The predominant mechanism that governs heating power is the mechanism which induces the most rapid variations of the magnetic moment. Absorption of magnetic energy is maximum when the characteristic time of fluctuations is close to the period of the excitation field ($\omega\tau \approx 1$) and SLP is proportional to the absorption rate multiplied by the frequency of the excitation field. Theoretical calculation predicts a nonmonotonous behavior of SLP as a function of particle size, with a sharp maximum associated with the Néel contribution and with a decrease for large diameters [2, 8]. For maghemite particles and assuming a volume anisotropy constant $K = 1.6 \times 10^4$ J m^{-3}, this maximum is found for a diameter of 14 nm (for a field frequency of 700 kHz). Beyond this optimum diameter, the SLP is expected to decrease with particle size. In parallel, the relative part of the Néel contribution to SLP diminishes in favor of the Brownian contribution. This nonmonotonous behavior is in quantitative agreement with the present experimental observations for the whole range of particle sizes (5–50 nm). The maximum of SLP (952 W g^{-1}) was found for polydisperse nanoparticles, with a characteristic major axis of 16 nm and minor axis of 12.8 nm. Moreover, our experimental results also highlight the different origins of heat generation for the whole range of particle sizes. The interplay between Néel and Brownian contributions was assessed by varying independently the particle size and the solvent viscosity. While both Brownian and Néel times are enhanced with particle size, the Néel time increased more rapidly, resulting in a crossover of Brownian and Néel regimes of heat generation. The Néel regime dominates for diameters below 20 nm (see figure 4(b)), whereas the Brownian regime prevails for larger diameters. Note that for maghemite nanoparticles, the high heating efficiency of particles with optimal diameter is primarily due to internal Néel dynamics. When Brownian dynamics begins to prevail, the global efficiency of heat generation is reduced.

Our results also assess, for the first time, the magnetic anisotropy of large diameter nonspherical maghemite nanoparticles. It was found that FMR behavior as well as hyperthermia measurements could be accounted for by a single value of volume anisotropy, for particles up to 20 nm. Beyond this size, FMR spectra disclose abnormally high anisotropy fields. Sources of additional anisotropy were not identified in this work, but could originate eventually from shape effects (although the eccentricity remains constant for all the samples) or from changes in crystalline structure depending on the synthesis parameters.

In conclusion, this parametric study provides a comprehensive investigation of the heating efficiency of γ-Fe_2O_3 nanoparticles as a function of their size in the range 5–50 nm. To our knowledge, it is the first time that such a large range of sizes has been investigated, combining FMR, dynamic birefringence experiments, and calorimetric measurements. The specific loss power of maghemite nanoparticles behaves as predicted theoretically, showing a maximum for an optimal particle size. The intricate contributions of Néel and Brownian mechanisms were identified and the balance between these two contributions was assessed in the whole size range.

Acknowledgments

We thank S de Montredon and S Neveu for the synthesis of the particles, J Servais and G Frasca for technical assistance, and INTAS (grant 03-51-6064) for financial support.

References

[1] Jordan A, Wust P, Fahling H, John W, Hinz A and Felix R 1993 *Int. J. Hyperth.* **9** 51–68
[2] Fortin J P, Wilhelm C, Servais J, Menager C, Bacri J C and Gazeau F 2007 *J. Am. Chem. Soc.* **129** 2628–35
[3] Massart R 1981 *IEEE Trans. Magn.* **17** 1247–8
[4] Daou T J, Pourroy G, Bégin-Colin S, Grenèche J M, Ulhaq-Bouillet C, Legaré P, Bernhardt P, Leuvrey C and Rogez G 2006 *Chem. Mater.* **18** 4399–404
[5] Wilhelm C, Gazeau F, Roger J, Pons J N, Salis M F, Perzynski R and Bacri J C 2002 *Phys. Rev.* E **65** 031404
[6] Gazeau F, Shilov V, Bacri J C, Dubois E, Gendron F, Perzynski R, Raikher Y L and Stepanov V I 1999 *J. Magn. Magn. Mater.* **202** 535–46
[7] Raikher Yu L and Shliomis M I 1994 *Advances in Chemical Physics: Relaxation Phenomena in Condensed Matter* vol 87 , ed W Coffey (New York: Wiley) pp 595–751
[8] Rosensweig R E 2002 *J. Magn. Magn. Mater.* **252** 370–4